PROCEEDINGS A

royalsocietypublishing.org/journal/rspa

Research

Cite this article: Califano F, Ciambella J. 2023 Viscoplastic simple shear at finite strains. *Proc. R. Soc. A* **479**: 20230603.
https://doi.org/10.1098/rspa.2023.0603

Received: 19 August 2023
Accepted: 17 November 2023

Subject Areas:
mechanical engineering, applied mathematics, civil engineering

Keywords:
viscoplasticity, viscoelasticity, torsion, pure shear

Author for correspondence:
J. Ciambella
e-mail: jacopo.ciambella@uniroma1.it

THE ROYAL SOCIETY PUBLISHING

Viscoplastic simple shear at finite strains

F. Califano[1] and J. Ciambella[2]

[1]Department of Mechanical and Aeronautical Engineering , and [2]Department of Structural and Geotechnical Engineering, Sapienza University of Rome, Rome, Italy

FC, 0000-0002-3471-2853; JC, 0000-0002-7498-5821

The equations governing the simple shear deformation of an incompressible inelastic material undergoing finite strain are derived in this paper. The constitutive assumptions are kept in their most general form to allow the incorporation of widely used viscoplastic or viscoelastic models from the literature. It is shown that, while for a hyperelastic material the simple shear problem is completely determined by a single parameter, the amount of shear, in the viscoplastic case, the elastic deformation is the superposition of a triaxial stretch and a simple shear, whose determination requires the solution of three coupled nonlinear evolution equations. We evaluate such a solution for different material models and compare it with three-dimensional finite element simulations to assess its accuracy. We further assess the performance of these models using experimental data from filled rubber, focusing on their ability to capture the observed behaviour, such as the well-known Payne effect. Additionally, we extend our simple shear solution to address torsion and the extension of thin-walled cylinders. These derivations and analyses offer valuable insights for experimentalists engaged in the mechanical characterization of soft materials.

1. Introduction

A simple shear deformation is a type of homogeneous deformation that preserves the volume and the normal direction of a plane, while altering the in-plane principal strain directions. The motion is usually applied by sliding the parallel faces of a parallelogram-shaped specimen while maintaining a constant distance between the plates. This type of deformation is extensively used to characterize materials spanning multiple length scales, from elastomers [1] to soft tissues [2] to granular materials [3] and geo-materials, due to the

multiple advantages this experimental setup offers over other tests. In simple tension and compression tests, stresses are uniform only in the central part of the sample, making it challenging to measure the corresponding deformations accurately. However, in simple shear experiments, by selecting an appropriate aspect ratio for the specimen, edge effects can be minimized and the stress field approximated as uniform within most of the sample volume [4]. Furthermore, simple shear experiments allow for varying the strain rate and confining pressure to simulate a range of loading conditions, providing insight into how material microstructure evolves under different external conditions [5].

Starting from the seminal work of Rivlin [6], extensive research has been conducted on simple shear for homogeneous isotropic elastic solids at large strain. This has resulted in a vast body of literature, as seen in works such as [7–10] and the references therein. When considering finite elasticity, the nature of simple shear deformation becomes complex and deviates from pure shear observed in the small strain regime [11,12]. Furthermore, the absence of fixed principal strain directions gives rise to various intriguing phenomena, one of which is the need for normal forces to maintain a constant distance between the sliding faces of the specimen [13]. This phenomenon, commonly referred to as Poynting's effect, can manifest in either a positive manner, causing the parallel faces to move apart, or a negative manner, causing them to come closer together [14]. Experimental evidence on negative Poynting's effect has been documented in hydrogels [15] and fibre-reinforced soft tissues [16], where it is induced by the relative inextensibility of the fibres in comparison to the matrix.

Simple shear deformation is also used to study the behaviour of inelastic materials, whose response depends not only on applied stresses but also on the rate of deformation and loading history [17,18]. For these materials, either constant strain rate tests or cyclic experiments are typically performed to assess rate dependence or hysteresis in stress–strain curves, respectively [19]. The models used to fit the experimental data can be either viscoelastic, viscoplastic or plastic.

One of the challenges in modelling viscoplastic simple shear is to ensure the well-posedness of the problem, which means that the solution exists, is unique and depends continuously on the initial and boundary data. However, many nonlinear viscoelastic models, such as the Oldroyd-B or the FENE-P models, are known to exhibit ill-posedness in simple shear, leading to unphysical singularities or multiple solutions [20,21]. To overcome this difficulty, some authors have proposed to introduce internal variables that account for the microstructural evolution of the material under shear. For example, Tzavaras [22] developed a general framework for materials with internal variables and relaxation of conservation laws, which ensures the well-posedness of the problem under certain conditions. He applied his theory to a class of viscoelastic fluids with fading memory and showed that the introduction of an internal variable related to the conformation tensor leads to a well-posed problem in simple shear.

When it comes to investigating inelastic simple shear deformation at large strains and fitting experimental data, the majority of studies rely on complex finite-element simulations to model the material behaviour and determine the constitutive parameters [23–25]. This approach can introduce additional challenges, particularly when attempting to solve the inverse problem of parameter identification. Consequently, the objective of this work is to develop a framework that allows for the derivation of the governing equations for a specimen undergoing large simple shear deformations using an inelastic material model, whether it be viscoplastic or viscoelastic. These equations will be obtained in closed form and solved numerically for different values of the constitutive parameters, providing a valuable alternative to the reliance on finite-element simulations.

Specifically, we will investigate how different material properties and boundary conditions influence the stress–strain response. Unlike in the elastic case, where the deformation is characterized by a single parameter (the amount of shear), the inelastic case requires determining up to three independent components of the elastic deformation by solving three coupled evolution equations. We will discuss some specific forms of these solutions that have been proposed previously and the constitutive assumptions required to obtain them.

In this sense, the paper extends previous literature results on simple shear in finite elasticity to finite inelasticity. In expanding on the primary understanding of simple shear deformation, moreover, this research examines scenarios combining simple shear with isochoric extension by focusing on the torsion of a thin-walled cylinder, which is another setup often used in experimental characterization of soft materials [26].

The structure of this paper is as follows. In §2, we establish a comprehensive three-dimensional framework for the inelastic model, with a specific focus on viscoelastic and viscoplastic behaviour. This general model is then further examined in the context of simple shear in §3. Section 4 explores the specific forms of the constitutive equations that emerge from this analysis. The subsequent sections address unique aspects of the model: §5 is dedicated to the study of extension and torsion of a thin-walled cylinder, while §6 delves into the model's behaviour under slow and fast deformations. Finally the numerical solutions of the problem and a comparison with fully three-dimensional FEM simulations are commented in §7. The appendix A is devoted to the discretization of the model for FE.

2. A review of the simple shear solution for incompressible materials in finite elasticity

In this section, we briefly review the simple shear solution in large strain elasticity. The interested reader is referred to Horgan & Murphy [10] and references therein. To describe the kinematics of hyperelastic materials, some basic concepts and notation have to be first defined. Let X be the coordinates of points in the reference configuration Ω, which is the undeformed state of the material. Let χ be the deformation map that assigns to each point X in Ω a point $x = \chi(X)$ in the current configuration Ω_t, which is the deformed state of the material. The deformation gradient $\mathbf{F} = \nabla\chi$ is a second-order tensor that measures the local change in length and orientation of material elements due to the deformation and $\mathbf{B}$ is the left-Cauchy Green strain tensor $\mathbf{B} = \mathbf{F}\mathbf{F}^T$. Throughout the text, a prime $'$ will be used to denote the deviatoric component of any tensor, that is $(\mathbf{A})' = \mathbf{A} - 1/3(\mathbf{A}\cdot\mathbf{I})\mathbf{I}$, where $\cdot$ is the inner product between tensors.

The constitutive equation of the Cauchy stress for an incompressible material is

$$\mathbf{T} = \mathbf{T}' - p\,\mathbf{I}, \tag{2.1}$$

where p is the Lagrange multiplier associated with the incompressibility constraint, i.e. $\det\mathbf{B} = 1$, and the deviatoric stress $\mathbf{T}'$ is constitutively assigned through the specific (per unit of mass) free energy density $\varphi(\mathbf{B})$. For isotropic materials, the strain energy density only depends on the invariants of the deformation tensor $\varphi = \phi(I_1, I_2)$ with

$$I_1 = \mathbf{I}\cdot\mathbf{B} \quad \text{and} \quad I_2 = \mathbf{I}\cdot\mathbf{B}^{-1}. \tag{2.2}$$

On defining, $\varphi_i = \rho\,\partial\phi/\partial I_i$, one has

$$\mathbf{T}' = 2\rho\left(\frac{\partial\varphi}{\partial\mathbf{B}}\mathbf{B}\right)' = 2\varphi_1\mathbf{B}' - 2\varphi_2(\mathbf{B}^{-1})'. \tag{2.3}$$

Simple shear-like motion in the $\mathbf{e}_1$–$\mathbf{e}_2$ plane is defined by

$$\mathbf{B} = \mathbf{I} + \gamma^2\mathbf{e}_1\otimes\mathbf{e}_1 + \gamma(\mathbf{e}_1\otimes\mathbf{e}_2 + \mathbf{e}_2\otimes\mathbf{e}_1), \tag{2.4}$$

where γ is the amount of shear. The constitutive equation (2.3) applied to the simple shear motion (2.4) yields the following result for the deviatoric part of the Cauchy stress

$$\left.\begin{aligned} T'_{11} &= \frac{2}{3}(2\varphi_1 + \varphi_2)\,\gamma^2,\\ T'_{22} &= -\frac{2}{3}(\varphi_1 + 2\varphi_2)\,\gamma^2\\ \text{and}\qquad T'_{12} &= 2(\varphi_1 + \varphi_2)\,\gamma, \end{aligned}\right\} \tag{2.5}$$

where $T'_{ij} = \mathbf{T}'\,\mathbf{e}_i \cdot \mathbf{e}_j$ and $T'_{33} = -T'_{11} - T'_{22}$.

Typically, constraints on the constitutive functions φ_1 and φ_2 are expressed through the well-known 'empirical inequalities':

$$\varphi_1 > 0 \quad \text{and} \quad \varphi_2 \geq 0. \tag{2.6}$$

Alternatively, a less restrictive set of constraints, known as the Baker–Ericksen inequalities, can be used. These inequalities are derived from the observation that the principal stress is greater in the direction of the greater principal stretch [27]. In addition, from experimental data on elastomer materials it is reasonable to expect that

$$\varphi_1 > 0 \quad \text{and} \quad \varphi_1 + \varphi_2 \geq 0. \tag{2.7}$$

In the case of an incompressible material, the empirical inequalities (2.6) imply the Poynting's effect to be positive [13], meaning that $T_{22} \leq 0$. This indicates a tendency for the parallel faces of the specimen to spread apart under simple shear deformation.

To determine the unknown pressure field p in the total stress $\mathbf{T}$, appropriate boundary conditions must be specified. Typically, two common boundary conditions are considered: *plane stress* and *zero normal traction* on the inclined faces. In the case of *plane stress*, it is assumed that the stress state is confined to a plane, meaning that there is no stress variation in the thickness direction of the material. This condition is often applied when the specimen is much thinner compared to the other dimensions of interest. Alternatively, the *zero normal traction* boundary condition implies that there is no normal force acting on the inclined faces of the material. The choice between these two boundary conditions depends on the specific problem being analysed.

(a) Plane stress

Plane stress boundary conditions assume that the material is subjected to external forces that act parallel to the plane of the sheared sample. This type of boundary condition has been widely used in experimental and theoretical studies of materials under simple shear deformation, including studies on granular materials and polymers. The condition of plane stress implies

$$\mathbf{T}\,\mathbf{e}_3 \cdot \mathbf{e}_3 = 0, \tag{2.8}$$

which upon substitution in (2.1) and on using of (2.5) gives the following expression of the reactive pressure p

$$p = \frac{2}{3}(-\varphi_1 + \varphi_2)\,\gamma^2, \tag{2.9}$$

needed to maintain the plane stress condition.

As a consequence the normal components of the Cauchy stress $\mathbf{T}$ are

$$\left.\begin{aligned} T_{11} &= 2\,\varphi_1\,\gamma^2 \\ \text{and} \qquad T_{22} &= -2\,\varphi_2\,\gamma^2 \end{aligned}\right\} \tag{2.10}$$

which shows that the normal stress component acting between the sliding faces T_{22} responsible for the so-called Poynting's effect is only present when the elastic energy does depend on the invariant I_2. Moreover, Poynting's effect can only be reverted if $\varphi_2 \leq 0$ meaning that the (2.6) are violated, yet it must be $\varphi_1 + \varphi_2 \geq 0$.

(b) Zero normal traction

Vanishing forces on the slanted faces boundary conditions are frequently used to simulate a free surface where the material is unconstrained in the direction perpendicular to the shear plane.

The stress vector acting on the slanted face is $\mathbf{Tn}$ with $\mathbf{n} = \mathbf{F}^*\mathbf{e}_1/|\mathbf{F}^*\mathbf{e}_1| = (1+\gamma^2)^{-1/2}(\mathbf{e}_1 - \gamma\,\mathbf{e}_2)$. In particular, the normal and the shear components of the Cauchy stress are

$$N = \mathbf{Tn}\cdot\mathbf{n}, \qquad \text{and} \qquad S = \mathbf{Tn}\cdot\mathbf{m}, \tag{2.11}$$

with $\mathbf{m} = (1+\gamma^2)^{-1/2}(\gamma\,\mathbf{e}_1 + \mathbf{e}_2)$. These lead to

$$S = \frac{T_{12}}{1+\gamma^2} \quad \text{and} \quad N = T'_{22} - p - \gamma\,S. \tag{2.12}$$

When no forces act on the slanted faces, $N = 0$ and $S = 0$. To determine the reactive pressure p that satisfies the first condition, equation $(2.12)_2$ is employed. Regarding the second condition, $S = 0$, equation $(2.12)_1$ reveals that sustaining the simple shear deformation invariably necessitates the presence of a shear stress at the boundary, unless both T_{12} and consequently γ are zero.

By incorporating the constitutive equations (2.5) into (2.12) and using the pressure expression obtained from the condition $N = 0$, the corresponding stress components can be derived as follows:

$$T_{11} = \frac{2\gamma^2}{1+\gamma^2}(\varphi_1+\varphi_2)(2+\gamma^2) \tag{2.13}$$

and

$$T_{22} = \frac{2\gamma^2}{1+\gamma^2}(\varphi_1+\varphi_2) = \frac{T_{11}}{2+\gamma^2}, \tag{2.14}$$

which shows that in absence of normal forces the Poyting's effect has a reverse sign ($T_{22} > 0$) since $\varphi_1 + \varphi_2 > 0$, meaning that the sliding faces would come closer together.

3. Inelastic model formulation

In the previous section, the equation governing the mechanical response of an elastic incompressible material undergoing simple shear deformation was derived. However, for many materials, the elastic model may not be sufficient to capture their complex deformation behaviour [28]. Therefore, in this section, we introduce a large strain inelastic model that extends the previous results to incorporate inelastic effects. The complexity of the material response requires the introduction of additional degrees of freedom, defined through an elastic *distortional* deformation tensor $\mathbf{B}_\mathrm{e}$, such that $\det\mathbf{B}_\mathrm{e} = 1$, which in the present formulation is an internal-like variable [29].

We postulate the standard principle of balance of linear momentum

$$\operatorname{div}\mathbf{T} + \mathbf{b} = \mathbf{0} \quad \text{and} \quad \mathbf{Tn} = \mathbf{t}, \tag{3.1}$$

with $\mathbf{b}$, $\mathbf{t}$ the forces per unit of (deformed) volume and area, respectively, and we set $\mathbf{b} = \mathbf{0}$ for the simple shear problem. Since only incompressible materials are considered in the present development, the Cauchy stress follows the split in equation (2.1) in which p is the reactive stress associated with the incompressibility constraint $\det\mathbf{B} = 1$.

The present inelastic theory requires the following constitutive equations to be specified at each material point

$$\mathbf{T}' = \widehat{\mathbf{T}}'(\mathbf{B}, \mathbf{B}_\mathrm{e}) \quad \text{and} \quad \dot{\mathbf{B}}_\mathrm{e} = \widehat{\dot{\mathbf{B}}}_\mathrm{e}(\mathbf{B}, \mathbf{B}_\mathrm{e}), \tag{3.2}$$

where $\widehat{\mathbf{T}}'$ is the constitutive equation of the deviatoric Cauchy stress and $\widehat{\dot{\mathbf{B}}_\mathrm{e}}$ is an evolution equation for an elastic deformation tensor that includes a rate of inelasticity. Here and henceforth a superimposed dot will be used to indicate material differentiation with respect to time.

The evolution equation of the elastic distortional strain can be alternatively expressed as

$$\dot{\mathbf{B}}_\mathrm{e} = \mathbf{L}'\mathbf{B}_\mathrm{e} + \mathbf{B}_\mathrm{e}\mathbf{L}'^{T} + \mathbf{B}_\mathrm{e}^{\nabla}, \tag{3.3}$$

emphasizing that $\mathbf{B}_\mathrm{e}$ does not evolve affinely with the total deformation $\mathbf{B}$, unless $\mathbf{B}_\mathrm{e}^{\nabla}$ is zero.[1] Equation (3.3) shows that specifying a constitutive equation for inelastic strain rate necessitates

[1]In fact if $\bar{\mathbf{B}} = (\det\mathbf{B})^{-1/3}\mathbf{B}$, $\dot{\bar{\mathbf{B}}} = \mathbf{L}'\bar{\mathbf{B}} + \bar{\mathbf{B}}\mathbf{L}'^{T}$. So, if $\mathbf{B}_\mathrm{e}^{\nabla} = 0$, $\mathbf{B}_\mathrm{e}$ evolves like $\bar{\mathbf{B}}$ [30].

defining a constitutive equation for $\mathbf{B}_e^{\nabla}$, that is often referred to as the 'codeformational derivative' of $\mathbf{B}_e$ [31]. To ensure that $\mathbf{B}_e$ remains unimodular, one must have $\dot{\mathbf{B}}_e \cdot \mathbf{B}_e^{-1} = 0$, that implies that the constitutive choice for $\mathbf{B}_e^{\nabla}$ must satisfy

$$\mathbf{B}_e^{\nabla} \cdot \mathbf{B}_e{}^{-1} = 0. \tag{3.4}$$

It is worth noting that definitions alternative to (3.3) were proposed in the literature by making use of Cotter–Rivlin or Jaumann derivatives (refer to Farina *et al.* [32] for a recent review). However, it should be emphasized that these alternative rates do not necessarily ensure that the evolution of $\mathbf{B}_e$ aligns with that of the total deformation $\mathbf{B}$ when the inelastic rate approaches zero.

In order to introduce constitutive prescriptions compatible with thermodynamics, we follow the Colemann–Noll procedure requiring the dissipation to be positive for each admissible thermodynamic process:

$$\rho\,\delta = \mathbf{T} \cdot \mathbf{D} - \rho\,\dot{\varphi} \geqslant 0, \tag{3.5}$$

where δ is the *specific* (per unit of mass) dissipation density, φ the specific elastic energy density and $\mathbf{D}$ the symmetric part of the velocity gradient $\mathbf{L} = \dot{\mathbf{F}}\mathbf{F}^{-1}$.

In the subsequent analysis, in accordance with the constitutive assumptions (3.2), it is presumed that the specific energy density solely depends on the elastic deformation, i.e. $\varphi = \widehat{\varphi}(\mathbf{B}_e)$. While some models in the literature decompose the energy into two additive terms—the equilibrium energy, dependent upon the total deformation $\mathbf{B}$, and the non-equilibrium energy, dependent upon the elastic deformation $\mathbf{B}_e$—this study focuses on the inelastic behaviour, neglecting the equilibrium energy. Its inclusion in the model is feasible [33], but its omission does not alter the primary focus on inelastic behaviour, leading to the designation of the developed material model as viscoplastic in this context.

Frame invariance requires the strain energy density to depend on the elastic strain invariants only:

$$\varphi = \phi(I_1^e, I_2^e), \tag{3.6}$$

defined by

$$I_1^e = \mathbf{I} \cdot \mathbf{B}_e, \quad \dot{I}_1^e = \mathbf{I} \cdot \dot{\mathbf{B}}_e = 2\,\mathbf{B}_e{}' \cdot \mathbf{D} + \mathbf{I} \cdot \mathbf{B}_e{}^{\nabla}$$

and

$$I_2^e = \mathbf{I} \cdot \mathbf{B}_e{}^{-1}, \quad \dot{I}_2^e = \mathbf{I} \cdot \dot{\mathbf{B}}_e^{-1} = -\mathbf{I} \cdot (\mathbf{B}_e{}^{-1}\dot{\mathbf{B}}_e\mathbf{B}_e{}^{-1}) = -2(\mathbf{B}_e{}^{-1})' \cdot \mathbf{D} - \mathbf{B}_e{}^{-2} \cdot \mathbf{B}_e^{\nabla}.$$

Accordingly, the material time derivative of the strain energy density gives

$$\rho\dot{\varphi} = 2[\varphi_1\,\mathbf{B}_e{}' - \varphi_2(\mathbf{B}_e{}^{-1})'] \cdot \mathbf{D} + (\varphi_1\,\mathbf{I} - \varphi_2\,\mathbf{B}_e{}^{-2}) \cdot \mathbf{B}_e^{\nabla}, \tag{3.7}$$

where the subscripts $_1$ or $_2$ denote the derivatives with respect to the first or second invariants, respectively, i.e. $\varphi_i = \rho\,\partial\phi/\partial I_i^e$. Introduction of (3.7) into the dissipation inequality (3.5) yields

$$\rho\,\delta = (\mathbf{T}' - 2\,\varphi_1\,\mathbf{B}_e{}' + 2\,\varphi_2(\mathbf{B}_e{}^{-1})') \cdot \mathbf{D} + \big(-\varphi_1\,\mathbf{I} + \varphi_2\,\mathbf{B}_e{}^{-2}\big) \cdot \mathbf{B}_e^{\nabla} \geqslant 0. \tag{3.8}$$

By assumption, a positive dissipation is associated with viscous losses and only the last term contributes to the irreversible processes, i.e. can have a positive dissipation. Therefore, the first term defines the constitutive equation for the Cauchy stress

$$\mathbf{T}' = 2\,\varphi_1\mathbf{B}_e' - 2\,\varphi_2(\mathbf{B}_e^{-1})', \tag{3.9}$$

that generalizes the elastic constitutive equation (2.3) to the present inelastic case. The second term in (3.8) describes the viscous dissipation, that can model the energy loss due to internal friction

Table 1. Viscoplastic/viscoelastic models from the literature incorporated in the proposed framework. In the table, we have defined quantities $J_1 = \mathbf{B} \cdot \mathbf{B}_e{}^{-1}$ and $J_2 = ||\mathbf{T}'||$.

	constitutive model	viscosity η
1	Reese & Govindjee [33]	*constant*
2	Bergström & Boyce [34]	$J_2^{1-m}/A(\overline{\lambda^v} - 1 + \xi)^c$ with $\overline{\lambda^v} = \sqrt{J_1/3}$
3	Kumar & Lopez-Pamies [35]	$(1/2)(\eta_\infty + ((\eta_0 - \eta_\infty + K_1[J_1^{\beta_1} - 3^{\beta_1}])/(1 + (K_2 J_2^2)^{\beta_2})))$
4	Strain hardening power law [36]	$J_2/\dot{\bar{\varepsilon}}^{cr}$ with $\dot{\bar{\varepsilon}}^{cr} = (AJ_2^n[(m+1)\bar{\varepsilon}^{cr}]^m)^{1/(m+1)}$
5	Drozdov [37] and Pom–Pom model [38,39]	$c/\sqrt{2}\,||\mathbf{D}||$
6	Rubin & Papes [30]	$(4/3)(c/\Gamma)\, I_2^e$

and heat generation. The dissipation assumes the reduced form

$$\rho\,\delta = -(\varphi_1 \mathbf{I} - \varphi_2 \mathbf{B}_e{}^{-2}) \cdot \mathbf{B}_e{}^{\nabla} = -(\varphi_1 \mathbf{B}_e - \varphi_2 \mathbf{B}_e{}^{-1}) \cdot (\mathbf{B}_e{}^{\nabla} \mathbf{B}_e{}^{-1}) \geq 0, \tag{3.10}$$

that by using (3.9) can be expressed directly in terms of the Cauchy stress as

$$\rho\,\delta = \mathbf{T}' \cdot \left(-\frac{1}{2}\,\mathrm{sym}(\mathbf{B}_e{}^{\nabla} \mathbf{B}_e{}^{-1}) \right) \geq 0. \tag{3.11}$$

To achieve standard smooth viscoplasticity, a quadratic form of the dissipation function in terms of the elastic stretch rate is usually assumed. Since the reduced dissipation in (3.11) is expressed in terms of deviatoric tensors, one can assume that the inelastic rate satisfies:

$$\frac{1}{2}\,\mathrm{sym}(\mathbf{B}_e{}^{\nabla} \mathbf{B}_e{}^{-1}) = -\frac{1}{\eta(\mathbf{B}, \mathbf{B}_e)} \mathbf{T}', \tag{3.12}$$

where η is the viscosity function that in general may depend on the total as well as the elastic strains. It should be noted that alternative constitutive choices can also be considered to satisfy (3.11). Nevertheless, the form (3.12) has the advantage of accommodating most of the viscoplastic models commonly employed in the literature.

Equation (3.12) demonstrates that at stationarity, when both $\dot{\mathbf{B}}_e$ and $\mathbf{L}$ are zero, and so is $\mathbf{B}_e{}^{\nabla}$, such as in the case of a relaxation test, the stress $\mathbf{T}'$ becomes zero and the material fully relaxes like a inviscid fluid. However, if a term in the energy dependent or the entire deformation $\mathbf{B}$ is included, the stress cannot reach zero during a relaxation test, which aligns with the expected behaviour of viscoelastic materials. It is important to note that this additional term in the energy only affects the steady-state behaviour and not the evolution problem. The proposed framework and constitutive assumptions are kept as general as possible to incorporates the vast majority of viscoplastic models used in the literature and listed in table 1.

Beyond the assumption about the specific energy density, models can be distinguished only by the form of the viscosity function. It was highlighted how elastomers display deformation-induced shear thinning. In this context, the viscosity function η is not constant (as seen in the Reese and Govindjee formulation, referred to as Model 1 in the table) but rather increases with applied deformation and decreases with the deformation rate. In order to describe this behaviour, Kumar and Lopez-Pamies (Model 3) use a viscosity function η that increases with J_1 (a measure of applied deformation) and decreases with J_2 (a measure of deformation rate). Bergström and Boyce model, on the other hand, postulates that viscosity is dependent upon the magnitude of the deviatoric Cauchy stress. This stress measure indirectly reflects the strain rate and is grounded in a microstructural rationale for the constitutive parameters. More precisely, the model assumes that the constituent molecules have the capacity to undergo substantial conformational changes when subjected to creep loading.

It is important to highlight that not all models were given with a specific form for the strain energy function. For instance, in the work by Reese & Govindjee [33], no explicit form is prescribed for the function φ, while a constant viscosity function is used. Similarly, the strain

hardening power law implemented in Abaqus FEA [36], which falls within this framework, allows for an arbitrary elastic strain energy, while the viscosity evolves according to the specified differential equation. This framework accommodates various other models as well. For instance, Kim *et al.* [40] employ a generic power law for the hyperelastic part and a viscosity that evolves based on the rate of deformation. Another example is found in the work by Yoshida & Sugiyama [41], where the evolution equation of the internal variables is defined in terms of the logarithmic stretch in the material frame. These examples demonstrate the flexibility of the framework to accommodate different formulations within the parallel rheological framework.

4. Simple shear deformation

We consider a simple shear-like motion in the $\mathbf{e}_1 - \mathbf{e}_2$ plane, characterized by the deformation rate tensor:

$$\mathbf{L} = \dot{\gamma}\, \mathbf{e}_1 \otimes \mathbf{e}_2, \tag{4.1}$$

where $\dot{\gamma}$ represents the time derivative of the amount of shear γ and $\mathbf{L} = \dot{\mathbf{F}}\mathbf{F}^{-1}$. Our goal is to find an elastic strain $\mathbf{B}_\mathrm{e}$, the solution to the evolution equation (3.12), in the form

$$\mathbf{B}_\mathrm{e} = b_1\, \mathbf{e}_1 \otimes \mathbf{e}_1 + b_2\, \mathbf{e}_2 \otimes \mathbf{e}_2 + b_3\, \mathbf{e}_3 \otimes \mathbf{e}_3 + b_{12}(\mathbf{e}_1 \otimes \mathbf{e}_2 + \mathbf{e}_2 \otimes \mathbf{e}_1), \tag{4.2}$$

that represents a simple shear deformation superimposed upon a triaxial stretch. In order to maintain this elastic deformation isochoric, it is required that:

$$b_3 = (b_1 b_2 - b_{12}^2)^{-1}, \tag{4.3}$$

whereas the conditions

$$b_1 > 0, b_2 > 0 \quad \text{and} \quad b_{12}^2 < b_1 b_2, \tag{4.4}$$

ensure that $\mathbf{B}_\mathrm{e}$ is a positive definite tensor.

The three unknown functions $b_1(t)$, $b_2(t)$ and $b_{12}(t)$ in (4.2)–(4.3) are determined by solving the three ordinary differential equations obtained by specializing (3.9) and (3.12) to the chosen form of $\mathbf{B}_\mathrm{e}$, that yields

$$\left.\begin{aligned} \dot{b}_1 &= \frac{4A_1}{3\eta} + 2\,\dot{\gamma}\, b_{12}, \\ \dot{b}_2 &= \frac{4A_2}{3\eta} \\ \text{and} \qquad \dot{b}_{12} &= \frac{4A_{12}}{3\eta}\, b_{12} + \dot{\gamma}\, b_2 \end{aligned}\right\} \tag{4.5}$$

with the initial conditions $b_1(0)$, $b_2(0)$ and $b_{12}(0)$. The parameters A_1, A_2, A_{12} are given by

$$\left.\begin{aligned} A_1 &= (b_1(-2\,b_1 + b_2 + b_3) - 3\,b_{12}^2)\,\varphi_1 \\ &\quad - (b_1^2(b_2 + b_3) - b_1(b_{12}^2 + 2\,b_2\,b_3) + 3\,b_{12}^2\,b_3)\,\varphi_2, \\ A_2 &= (b_2(b_1 - 2\,b_2 + b_3) - 3\,b_{12}^2)\,\varphi_1 \\ &\quad - (b_2\,(b_1(b_2 - 2b_3) + b_2\,b_3) - b_{12}^2(b_2 - 3\,b_3))\,\varphi_2 \\ \text{and} \qquad A_{12} &= (b_3 - 2\,b_1 - 2\,b_2)\,\varphi_1 - \frac{1}{b_3}(b_1\,b_3^2 + b_2\,b_3^2 + 1)\,\varphi_2 \end{aligned}\right\} \tag{4.6}$$

and depend on the specific form of the constitutive equations enforced (table 1). It is noted that η may depend on the elastic or macroscopic strains as well.

The constitutive equation of the Cauchy stress specialized with (4.2) gives the following non-zero stress components:

$$\left.\begin{aligned} T'_{11} &= \frac{2}{3}(2b_1 - b_2 - b_3)\varphi_1 + \frac{2}{3}(b_1 - 2b_2)b_3\varphi_2 + \frac{2\varphi_2}{3b_3}, \\ T'_{22} &= \frac{2}{3}(2b_2 - b_1 - b_3)\varphi_1 + \frac{2}{3}(b_2 - 2b_1)b_3\varphi_2 + \frac{2\varphi_2}{3b_3} \\ \text{and} \quad T'_{12} &= 2b_{12}(\varphi_1 + b_3\varphi_2), \end{aligned}\right\} \tag{4.7}$$

with b_3 given in equation (4.3) and $T'_{33} = -T'_{11} - T'_{22}$.

As discussed in §7, at extremely high shear rates, the response of this inelastic model coincides with that of the hyperelastic model. Consequently, it is expected that the constitutive coefficients φ_1 and φ_2 will adhere to either the Baker–Ericksen inequalities or the more restrictive empirical inequalities.

Obtaining an analytical solution for the nonlinear evolution equations (4.5) becomes tractable in certain simplified scenarios. For instance, under conditions of small strains, the model simplifies to the standard rheological Maxwell model, allowing for analytical integration over time. Additionally, specific constitutive assumptions can lead to the derivation of closed-form steady-state solutions, particularly when the deformation rate approaches zero. An illustrative example of this is found in the [30] model, where such a solution was obtained under the context of monotonic loading with a constant shear rate.

(a) Rivlin's universal relation

Rubin & Chen [42] showed that a viscoplastic material of the type discussed in this paper satisfies the relationship

$$\mathbf{T}\mathbf{B}_{\mathrm{e}} = \mathbf{B}_{\mathrm{e}}\mathbf{T}, \tag{4.8}$$

which is a consequence of the fact that $\mathbf{B}_{\mathrm{e}}$ and $\mathbf{T}$ have the same principal directions (see equation (3.9)). Equation (4.8) generalizes the well-known property of the Cauchy stress that for a hyperelastic material commutes with $\mathbf{B}$, i.e. $\mathbf{B}\mathbf{T} = \mathbf{T}\mathbf{B}$, and gives the celebrated Rivlin's universal relation for simple shear

$$T_{11} - T_{22} = \gamma\, T_{12}. \tag{4.9}$$

When equation (4.8) is valid, it leads to the following relationship between normal and shear stress components:

$$b_{12}(T_{11} - T_{22}) = (b_1 - b_2)\, T_{12}, \tag{4.10}$$

which is a *universal relation* within the class of viscoplastic materials considered in this paper. Its foundation lies in the fact that $\mathbf{B}_{\mathrm{e}}$ encompasses a simple shear deformation superimposed on a triaxial stretch. Notably, a relationship akin to equation (4.10) was previously discussed by Rajagopal and Wineman for hyperelastic materials in [43].

We further note that in order for (4.10) to give (4.9) one must have

$$b_1 - b_2 = \gamma\, b_{12}, \tag{4.11}$$

which implies $\dot{b}_1 - \dot{b}_2 = \dot{\gamma}\, b_{12} + \gamma\, \dot{b}_{12}$. Upon substituting the evolution equations (4.5) into the last expression, we find that it holds true if and only if the following relationships are satisfied:

$$b_1 = (1 + \gamma^2)\, b_2 \quad \text{and} \quad b_{12} = \gamma\, b_2. \tag{4.12}$$

This implies that the parameter b_2 is the only independent parameter in the elastic deformation. However, for this condition to be satisfied, the three evolution equations (4.5) must be linearly dependent, which is not the case except when $\eta \to \infty$. In such a scenario, the three evolution equations yield $\dot{b}_1 = \dot{b}_2 = \dot{b}_{12} = 0$, leading to the recovery of the hyperelastic model where Rivlin's relation holds true. In the general case, however, it should be noted that the relationship (4.9) cannot be fulfilled at every time instant, indicating that Rivlin's universal relation does not apply to the wide range of inelastic materials considered in this study.

(b) Plane stress

Upon imposing the plane stress condition $T_{33}=0$, the reactive pressure p can be determined from $T_{33}=-T'_{11}-T'_{22}-p=0$ as follows:

$$p=\frac{2}{3}\left(\varphi_2 b_3(b_1+b_2)+2\varphi_1 b_3-\varphi_1(b_1+b_2)-\frac{2\varphi_2}{b_3}\right). \tag{4.13}$$

As a consequence, the non-vanishing normal components of the Cauchy stress are:

$$\left.\begin{aligned} T_{11}&=2(b_1-b_3)\,\varphi_1+\left(\frac{2}{b_3}-2\,b_3\,b_2\right)\varphi_2\\ \text{and}\qquad T_{22}&=2(b_2-b_3)\,\varphi_1+\left(\frac{2}{b_3}-2\,b_3\,b_1\right)\varphi_2. \end{aligned}\right\} \tag{4.14}$$

Upon closer examination, the equations demonstrate that, unlike in the elastic case, the maintenance of deformation requires a normal force T_{22}, even for material models that do not depend on the I_2^e invariant (for which $\varphi_2=0$). By contrast, in the hyperelastic case, such a force was not present. This phenomenon can be interpreted as an inelastic manifestation of the Poynting's effect.

(c) Zero normal traction

With the constitutive equation (4.7), by applying (2.11), one can work out the normal and shear forces acting on the inclined faces. These read as

$$S=\frac{T_{12}}{1+\gamma^2}\left(1-\gamma^2+\gamma\frac{b_1-b_2}{b_{12}}\right) \tag{4.15}$$

and

$$N=T'_{22}-p+\frac{T_{12}}{1+\gamma^2}\left(\frac{b_1-b_2}{b_{12}}-2\,\gamma\right), \tag{4.16}$$

with $T_{12}=2\,b_{12}(\varphi_1+b_3\varphi_2)$. By imposing a vanishing normal component $N=0$, one can calculate the value of the reacting pressure:

$$p=T'_{22}+\frac{T_{12}}{1+\gamma^2}\left(\frac{b_1-b_2}{b_{12}}-2\,\gamma\right), \tag{4.17}$$

that give the following expressions of the normal stress components:

$$\left.\begin{aligned} T_{11}&=\frac{\gamma\,T_{12}}{1+\gamma^2}\left(\frac{b_1-b_2}{b_{12}}\gamma+2\right)\\ \text{and}\qquad T_{22}&=-\frac{T_{12}}{1+\gamma^2}\left(\frac{b_1-b_2}{b_{12}}-2\,\gamma\right). \end{aligned}\right\} \tag{4.18}$$

When the response approach that of an elastic solid, $b_1\to 1+\gamma^2$, $b_2\to 1$ and $b_{12}\to\gamma$ and so equations (2.13) and (2.14) are recovered.

5. Specific forms of the constitutive equation

Within the aforementioned general framework, we now focus on specific solutions of the evolution equations that have been employed in the literature. We aim to elucidate the form of the strain energy density required to sustain such solutions. One of the distinctive characteristics of the simple shear deformation is that both strain invariants, I_1 and I_2, are equal and given by $3+\gamma^2$. This implies that in a simple shear-like motion, the energy density $\varphi(I_1,I_2)$ is evaluated on the bisector of the I_1-I_2 plane.

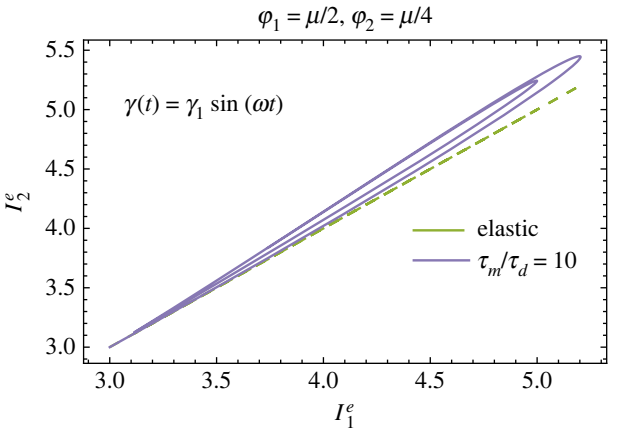

Figure 1. Elastic strain invariants I_1^e versus I_2^e during a simple shear test with a sinusoidal time law. The elastic energy is modelled using the Mooney–Rivlin constitutive equation with $\varphi_1 = \mu/2$ and $\varphi_2 = \mu/4$. The results illustrate the deviation from the elastic solution, represented by the dashed line.

In the viscoplastic case this is not necessarily the same in fact

$$I_1^e = b_1 + b_2 + b_3, \tag{5.1}$$

and

$$I_2^e = \frac{1}{b_3} + (b_1 + b_2)\, b_3 = I_1^e\, b_3 - b_3^2 + \frac{1}{b_3}. \tag{5.2}$$

These expressions demonstrate that, for the general form of $\mathbf{B}_e$ as given in (4.2), the two invariants are distinct and not equal to each other. This implies that during simple shear testing of this inelastic material, the elastic energy is evaluated over a larger portion of its domain, not confined to the bisectrix of the I_1^e–I_2^e plane. An illustrative example of this phenomenon is provided in figure 1, where γ follows a sinusoidal time law, and the material is modelled using a Mooney–Rivlin constitutive equation with $\varphi_1 = \mu/2$ and $\varphi_2 = \mu/4$. The results clearly demonstrate that during the test, the ratio between the two invariants deviates from the behaviour observed in the purely elastic case.

One may question whether it is possible to focus on a specific class of materials for which the solution of the evolution problem is such that $I_1^e = I_2^e$. By equalling (5.1) and (5.2), immediately follows that the two invariants coincide when

$$b_3 = 1, \tag{5.3}$$

that implies

$$b_1 = \frac{1 + b_{12}^2}{b_2}. \tag{5.4}$$

Substituting the solution (5.3) into the evolution equations (4.5), to guarantee the solvability of the system two of the three equations must be linearly dependent. This is true for a particular class of materials for which:

$$\varphi_1 = \varphi_2 \quad \text{and} \quad \eta \neq 0, \tag{5.5}$$

when $I_1^e = I_2^e$, implying that the elastic strain energy density has the same functional dependence on the first and second invariants. It is worth noting that a Neo-Hookean constitutive assumption would not fulfil this requirement, while a Mooney–Rivlin constitutive assumption with equal coefficient $c_{10} = c_{01}$ would satisfy it.

Under this circumstance the stress turns out to be

$$\left.\begin{aligned} T'_{11} &= \frac{2}{b_2}\,\varphi_1\,(1-b_2^2+b_{12}^2),\\ T'_{22} &= -\frac{2}{b_2}\,\varphi_1\,(1-b_2^2+b_{12}^2)\\ \text{and}\qquad T'_{12} &= 4\,\varphi_1\,b_{12}, \end{aligned}\right\} \tag{5.6}$$

where the elastic stretch components b_2 and b_{12} are determined by the evolution equations:

$$\dot{b}_2 = \frac{4\,\varphi_1}{\eta}\,(1-b_2^2-b_{12}^2), \tag{5.7}$$

and

$$\dot{b}_{12} = b_2\,\dot{\gamma} - \frac{4\,\varphi_1\,b_{12}}{\eta\,b_2}\,(1+b_2^2+b_{12}^2), \tag{5.8}$$

with the corresponding initial condition $b_2(0)=1$ and $b_{12}(0)=0$.

Interestingly the solution (5.6) implies the out-of-plane component T'_{33} to vanish, which is also true for the elastic solution (2.3) when $\varphi_1=\varphi_2$.

It is further noted that several papers in the open literature have made the more restrictive assumption that the elastic triaxial stretch vanishes. This assumption corresponds to a specific case of the solution (5.3), where an additional condition is imposed such that $b_2=1$, resulting in both $\mathbf{B}_{\mathrm{e}}$ and $\mathbf{B}$ having the same functional form (as seen in, for example, [44] where $b_{12}=\gamma_e$). However, it should be noted that this is not a solution of the evolution equations (4.5). Specifically, it can be observed that in such a case, $\dot{b}_2$ would need to be zero. However, based on (5.7), this condition can only be satisfied if $\varphi_1=0$, which together with the condition $\varphi_1=\varphi_2$, is clearly impossible.

6. Torsion and extension of a thin-walled incompressible cylinder

In this section, we study a thin-walled circular cylinder under the influence of both axial force and a twisting moment. Our objective here is to extend prior discussions by addressing a deformation that combines simple shear and isochoric extension. Such deformation configurations are frequently employed in experimental settings to effectively determine the constitutive parameters of hyperelastic models as an alternative to simple shear deformation (see, for instance, [26]). Furthermore, our analysis sheds light on the intricate relationship between constitutive parameters and the Poynting effect, as discussed in [43].

We consider a thin-walled cylinder with undeformed dimensions H_0, T_0 and R_0 ($T_0 \ll R_0$), representing height, thickness of the wall, and radius, respectively. To describe the motion of such a cylinder, we employ a cylindrical coordinate system in which $\mathbf{e}_3$ is the fixed cylinder axis, and $\mathbf{e}_r$ and $\mathbf{e}_\theta$ are the polar coordinates in the cross-section plane of the deformed configuration; we call $\{z(t),\theta(t),r(t)\}$ the coordinates of point p at time t. Accordingly, $\{\mathbf{E}_3,\mathbf{E}_\theta,\mathbf{E}_r\}$ are the reference axes with the corresponding referential coordinates given by $\{Z,\Theta,R\}$. With respect to the fixed orthonormal triad $\{\mathbf{e}_1,\mathbf{e}_2,\mathbf{e}_3\}$, one has

$$\mathbf{e}_r = \cos(\theta)\,\mathbf{e}_1 + \sin(\theta)\,\mathbf{e}_2 \quad \text{and} \quad \mathbf{e}_\theta = -\sin(\theta)\,\mathbf{e}_1 + \cos(\theta)\,\mathbf{e}_2,$$

such that $\dot{\mathbf{e}}_r = \dot{\theta}\,\mathbf{e}_\theta$ and $\dot{\mathbf{e}}_\theta = -\dot{\theta}\,\mathbf{e}_r$.

Accordingly, the motion of the cylinder is a one-to-one map that assigns at each point P in the reference configuration, a point p in the deformed configuration with coordinates

$$z(t) = \lambda(t)\,Z, \quad \theta(t) = \Theta + \phi(t)\,\frac{Z}{H_0}, \quad r = \frac{R}{\sqrt{\lambda(t)}}. \tag{6.1}$$

Here, λ represents the longitudinal stretch, while ϕ/H_0 denotes the relative torsion angle between the top and bottom faces of the cylinder, expressed per unit of reference height. We will consider two cases: one in which the torsion angle is prescribed and expansion along the

cylinder axis is hampered in a way that $\lambda(t) = 1$, by referring to it as *pure torsion*; the other in which the cylinder is let free to expand in the axis direction in a way that the normal force is zero; the additional hypothesis, that the cylinder is thin-walled, allows us to write previous condition locally as $T_{zz} = \mathbf{T}\mathbf{e}_3 \cdot \mathbf{e}_3 = 0$.

The deformation tensor in the cylindrical reference system resulting from the motion described in equation (6.1) is

$$\mathbf{F} = \lambda\, \mathbf{e}_3 \otimes \mathbf{E}_3 + \frac{1}{\sqrt{\lambda}}(\mathbf{e}_\theta \otimes \mathbf{E}_\Theta + \mathbf{e}_r \otimes \mathbf{E}_R) + \frac{\gamma}{\sqrt{\lambda}}\mathbf{e}_\theta \otimes \mathbf{E}_3, \quad \gamma = \frac{\kappa\, \phi\, R}{R_0}, \tag{6.2}$$

where we have defined the aspect ratio of the cylinder $\kappa = R_0/H_0$, and the shear strain γ that under the assumption that the cylinder is thin-walled, $R \simeq R_0$, is $\gamma \simeq \kappa\, \phi$. The tensor in (6.2) corresponds to a simple shear deformation with a shear component of γ superimposed on an isochoric extension with a magnitude λ. The deformation rate is non-homogeneous throughout the height and is expressed in terms of the normalized reference coordinate $\zeta = Z/H_0$, $\zeta \in [0, 1]$, as

$$\mathbf{L} = \frac{\dot{\lambda}}{\lambda}\left(\mathbf{e}_3 \otimes \mathbf{e}_3 - \frac{1}{2}\mathbf{e}_\theta \otimes \mathbf{e}_\theta - \frac{1}{2}\mathbf{e}_r \otimes \mathbf{e}_r\right) + \frac{\kappa\, \dot{\phi}}{\lambda^{3/2}}\, \mathbf{e}_\theta \otimes \mathbf{e}_3 + \zeta\, \dot{\phi}\, (\mathbf{e}_\theta \otimes \mathbf{e}_r - \mathbf{e}_r \otimes \mathbf{e}_\theta), \tag{6.3}$$

where, again, the fact that $R \simeq R_0$ was used. It is noted that the last component of the deformation rate represents an additional shearing velocity that arises in the problem due to the geometry of the specimen. Notably, it was not present in the previously studied simple shear case.

To solve the evolution problem (3.12), we follow the same semi-inverse approach used in the simple shear case by seeking for a solution of the evolution equation in the following form

$$\mathbf{B}_\mathrm{e} = b_z\, \mathbf{e}_3 \otimes \mathbf{e}_3 + b_\theta\, \mathbf{e}_\theta \otimes \mathbf{e}_\theta + b_r\, \mathbf{e}_r \otimes \mathbf{e}_r + b_{z\theta}(\mathbf{e}_3 \otimes \mathbf{e}_\theta + \mathbf{e}_\theta \otimes \mathbf{e}_3), \tag{6.4}$$

with only three independent components due to the constraint $\det \mathbf{B}_\mathrm{e} = 1$, e.g. $b_r = 1/(b_z\, b_\theta - b_{z\theta}^2)$. Consequently, the differential equations governing the evolution of the elastic variables, as derived from previous definitions, are

$$\left.\begin{aligned} \dot{b}_z &= \frac{4\, B_z}{3\, \eta} + 2\, \frac{\dot{\lambda}}{\lambda}\, b_z, \\ \dot{b}_\theta &= \frac{4\, B_\theta}{3\, \eta} - \frac{\dot{\lambda}}{\lambda}\, b_\theta + 2\, \frac{\kappa\, \dot{\phi}}{\lambda^{3/2}}\, b_{z\theta} \\ \text{and} \quad \dot{b}_{z\theta} &= \frac{4\, B_{z\theta}}{3\, \eta} b_{z\theta} + \frac{\dot{\lambda}}{2\, \lambda}\, b_{z\theta} + \frac{\kappa\, \dot{\phi}}{\lambda^{3/2}}\, b_z \end{aligned}\right\} \tag{6.5}$$

with

$$\left.\begin{aligned} B_z &= \left(b_z\, (b_r - 2\, (b_z + b_\theta)) + \frac{3}{b_r}\right)\, \varphi_1 + \left(3 - \frac{b_z}{b_r} - b_r b_z (b_z + b_\theta)\right)\, \varphi_2, \\ B_\theta &= \left(3 b_r b_{z\theta}^4 + (b_r + 4 b_z) b_\theta - (2 + 3 b_r b_z^2) b_\theta^2\right)\, \varphi_1 + \left(3 - 2 b_z b_\theta^2 - b_r b_\theta (b_z + b_{z\theta}^4 + b_\theta - b_z^2 b_\theta^2)\right) \varphi_2 \\ \text{and} \quad B_{z\theta} &= \left(b_r - 2\, (b_z + b_\theta)\right)\, \varphi_1 - \left(2 b_z b_\theta + b_r\, (b_z + b_{z\theta}^4 + b_\theta - b_z^2\, b_\theta^2),\right)\, \varphi_2. \end{aligned}\right\} \tag{6.6}$$

The integration of equation (6.5) is performed with the initial conditions $b_z(0) = b_\theta(0) = 1$ and $b_{z\theta}(0) = 0$, and upon substituting this solution into the constitutive equation (3.9), we obtain the expression for the deviatoric component of the Cauchy stress. The determination of the unknown pressure field $p(t)$, which is a result of the incompressibility constraint, is achieved by enforcing zero pressure on the external surface of the cylinder. This requirement, combined with the assumption of a thin-walled cylinder, results in the condition $T_{rr} = \mathbf{T} \cdot \mathbf{e}_r \cdot \mathbf{e}_r = 0$.

In §8, we present the numerical solution of equation (6.5) for both the pure torsion and zero normal force cases.

7. Limiting elastic and viscous behaviour

In the limiting cases of fast or slow deformations, the proposed viscoplastic model exhibits characteristics akin to those of an elastic solid or a viscous fluid, respectively. To explore this further, we analyse the response of the model under a constant shear rate deformation such that $\gamma = t/\tau_d$, where τ_d represents the characteristic time scale of the deformation, and $\dot{\gamma} = 1/\tau_d$ denotes the shear rate. Additionally, we introduce a relaxation time $\tau_m = \sup(\eta/\mu)$, where μ corresponds to the shear modulus of the material.

Upon a dimensionalization of the evolution equations, we obtain the following forms:

$$\left.\begin{aligned} b_1' &= \frac{4}{3}\frac{\tau_d}{\tau_m}\tilde{A}_1 + 2\,b_{12}, \\ b_2' &= \frac{4}{3}\frac{\tau_d}{\tau_m}\tilde{A}_2 \\ \text{and} \qquad b_{12}' &= \frac{4}{3}\frac{\tau_d}{\tau_m}\tilde{A}_{12}\,b_{12} + b_2. \end{aligned}\right\} \tag{7.1}$$

Here, a prime is used to indicate the derivative with respect to the dimensionless time t/τ_d, and the tilde indicates a dimensionalization with respect to μ.

(a) Fast shear rates

For fast shear rates one has $\tau_d/\tau_m \to 0$, the material undergoes rapid deformation, and the evolution equations simplify to:

$$b_1' = 2\,b_{12}, \quad b_2' = 0, \quad b_{12}' = b_2, \tag{7.2}$$

These equations can be integrated analytically with the initial conditions $b_1(0) = b_2(0) = 1$ and $b_{12}(0) = 0$, yielding:

$$b_1(t) = 1 + \gamma^2(t), \quad b_2(t) = 1, \quad b_{12}(t) = \gamma(t), \tag{7.3}$$

where $\gamma(t) = t/\tau_d$. It can be observed that $\mathbf{B}_\mathrm{e}$ coincides with $\mathbf{B}$, indicating that the material's response is equivalent to that of an elastic material.

(b) Slow shear rates

In the case of slow applied shear rates ($\tau_m/\tau_d \to 0$), the evolution equations reduce to the following system of algebraic equations:

$$\left.\begin{aligned} A_1(b_1, b_{12}, b_2) &= 0, \\ A_2(b_1, b_{12}, b_2) &= 0 \\ \text{and} \qquad A_{12}(b_1, b_{12}, b_2) &= 0. \end{aligned}\right\} \tag{7.4}$$

By employing the definitions (4.6), the only valid solution of this system $b_1 = b_2 = 1$ and $b_{12} = 0$, that means that the elastic deformation vanishes ($\mathbf{B}_\mathrm{e} = \mathbf{I}$), and the stress is zero. Therefore, under such slow deformation, the material flows at zero stress like a viscous fluid.

8. Numerical solution of the evolution problem

In this section, we provide some insight into the material behaviour by solving numerically the evolution problem for both simple shear and torsion cases. The analytical solution is compared with three-dimensional finite-element simulations to assess its accuracy for varying specimen geometry and with experimental data on filled rubber.

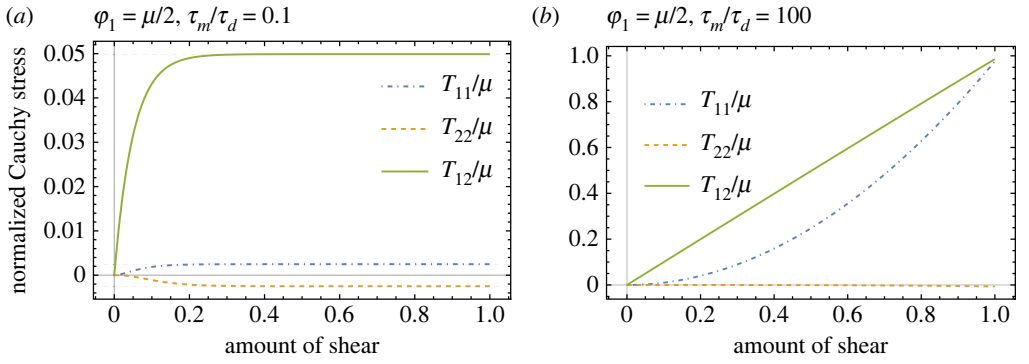

Figure 2. (Constant shear rate test) Normalized Cauchy stress components T_{11}/μ, T_{22}/μ, and T_{12}/μ as functions of shear amount γ for two different strain rates: $\tau_m/\tau_d = 1$ (*a*) and $\tau_m/\tau_d = 100$ (*b*) under plane stress condition. The elastic energy is Neo-Hooke with $\varphi = \mu/2$.

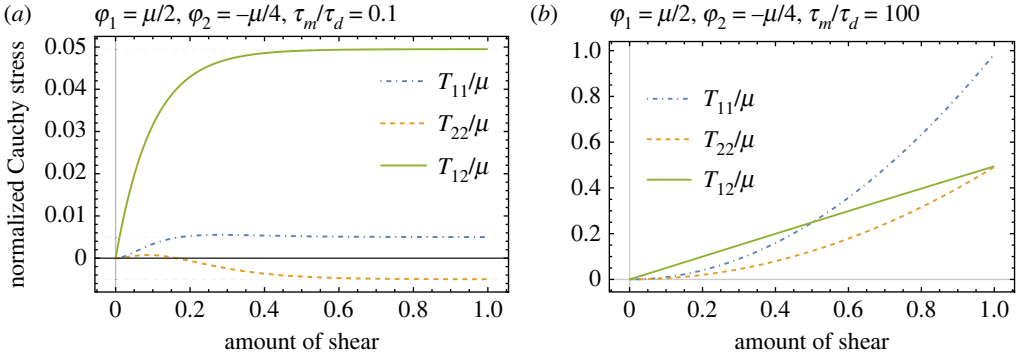

Figure 3. (Constant shear rate test) Normalized Cauchy stress components T_{11}/μ, T_{22}/μ and T_{12}/μ as functions of shear amount γ for two different strain rates: $\tau_m/\tau_d = 1$ (*a*) and $\tau_m/\tau_d = 100$ (*b*) under plane stress condition. The elastic energy is Mooney–Rivlin with $\varphi_1 = \mu/2$ and $\varphi_2 = -\mu/4$.

(a) Simple shear

We define the shear rate $\dot{\gamma}$ in equation (4.1) to be

$$\dot{\gamma} = \frac{1}{\tau_d},$$

with $1/\tau_d$ the constant shearing rate and

$$\dot{\gamma} = \begin{cases} \dfrac{1}{\tau_d}, & 0 \le t \le t_m \\ -\dfrac{1}{\tau_d}, & t_m \le t \le 2\,t_m, \end{cases}$$

for a cyclic test lasting $2\,t_m$. The elastic energy density is assumed to be either of Neo-Hookean type with $\varphi_1 = \mu/2$ (μ is the shear modulus) or of Mooney–Rivlin type with $\varphi_1 = \mu/2$ and $\varphi_2 = -\mu/4$, with this latter coefficient being negative to simulate a negative Poynting's effect. The viscosity function η is assumed to be constant and defined in terms of the shear modulus μ and a material time constant τ_m such that $\eta = \mu\tau_m$.

For a constant shear rate test with low rate ($\tau_m/\tau_d = 0.1$), both the Neo-Hooke figure 2*a* and the Mooney–Rivlin figure 3*a* models display the typical response of a viscoplastic material:

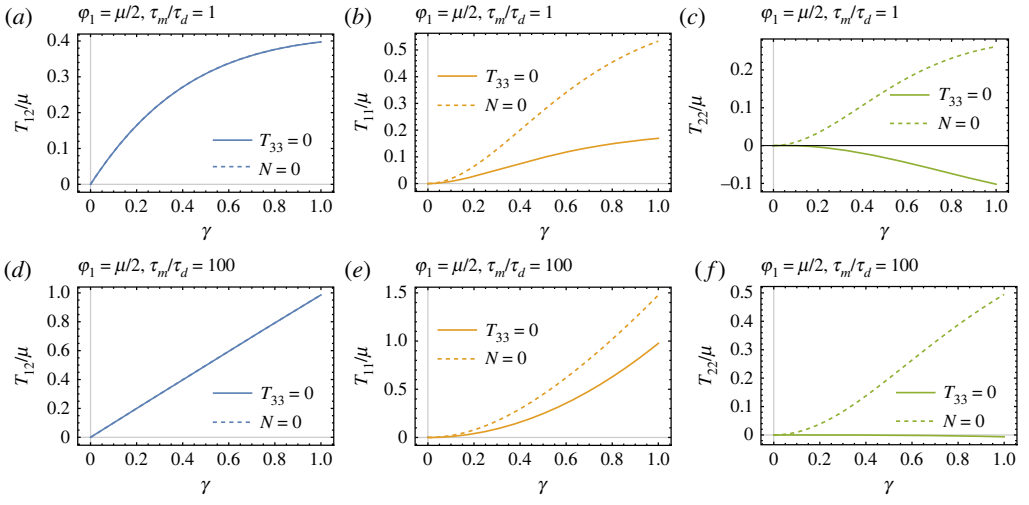

Figure 4. Effects of boundary conditions on the stresses for constant shear tests under plane stress ($T_{33} = 0$) and zero normal forces ($N = 0$). The elastic energy is Neo-Hooke with $\varphi = \mu/2$ and the characteristic time is $\tau_m/\tau_d = 1$ (*a*,*b*,*c*) and $\tau_m/\tau_d = 100$ (*d*,*e*,*f*).

the stress components increase with strain and then reach stationary values, indicating that the material flows at constant stress levels. It is noteworthy that the steady-state values of the component T_{22} are negative for both the models, indicating the tendency of the parallel faces of the specimen to expand (positive Poynting's effect). Although this is expected for the Neo-Hookean material model, the Mooney–Rivlin hyperelastic material with $\varphi_2 < 0$ should have a reversal of the Poytining effect with $T_{22} > 0$ (negative Poynting's effect) as equation (2.10.2) shows. In the viscoplastic case this is only true in the initial part of the loading curve for very short time (figure 3*a*), but at longer times, the sign of the Poynting's effect is reverted, meaning that the parallel faces which were initially contracted, start expanding.

When $\tau_m/\tau_d = 100$ in figures 2*b* and 3*b*, the experimental test is 'fast' and the material response approaches that of an elastic material and the relationship between the amount of shear γ and the shear stress T_{12} becomes almost linear, whereas the normal stress T_{11} is a quadratic function of γ. As for the hyperelastic Neo-Hookean model in plane stress, the component T_{22} is almost zero, and the Poynting's effect is absent, whereas the Mooney–Rivlin model displays the negative Poytning effect expected from the constitutive choice $\varphi_2 < 0$.

It is noted that the horizontal dashed lines in the figures represent the stationary values of the stresses obtained by numerically solving equation (7.1) with $b_1'(t) = b_2'(t) = b_{12}'(t) = 0$.

The comparison in figure 4 provides observations regarding the effects of different boundary conditions on stress evolution. The shear stress is unaffected by the boundary conditions as it is independent of pressure. Conversely, significant disparities emerge in the normal stress components, particularly T_{22}: when the material response exhibits viscoplastic behaviour (characterized by $\tau_m/\tau_d = 1$), T_{22} experiences a reversal between the plane stress and zero normal force conditions. However, as the response approaches the elastic Neo-Hooke model, T_{22} tends to converge to zero for plane stress.

The cyclic tests shown in figure 5 exhibit the characteristic hysteresis behaviour anticipated in a viscoplastic material model. When τ_m/τ_d is low, indicating that the deformation's characteristic time is longer than the material's time, the material undergoes steady flow at a constant stress. Upon unloading, the material experiences compression once more at a consistent shear stress level. The peak dissipation effect is most pronounced at $\tau_m/\tau_d = 1$, while larger values lead to a response that approaches that of an elastic material, characterized by considerably reduced hysteresis.

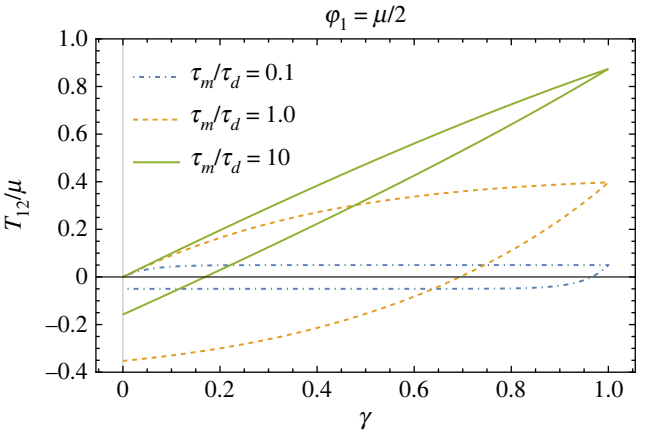

Figure 5. (Cyclic test) Normalized shear stress T_{12}/μ as a function of the amount of shear γ for cyclic tests under different strain rates: $\tau_m/\tau_d = \{0.1, 1, 10\}$.

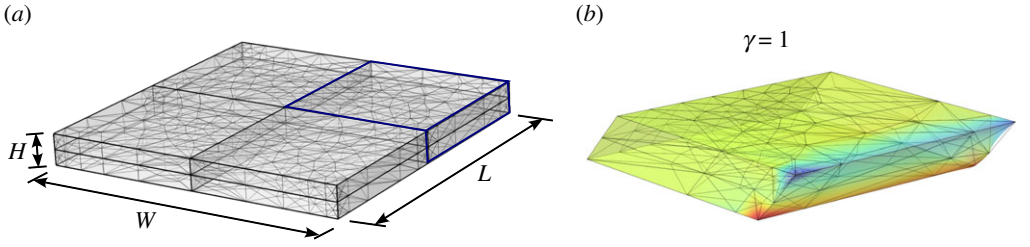

Figure 6. Reference specimen geometry used in FE to simulate the simple shear experiment (*a*). Details of a quarter of the specimen in the deformed configuration with $\gamma = 1$ (*b*) (the contour plot displays the reactive pressure field).

Table 2. Geometric and constitutive parameters used in the FE simulations

geometry	constitutive parameters
$H = 1$ mm	$\mu = 10$ MPa
$L = W = 10$ mm	$\eta = \mu\,\tau_m, \quad \tau_m = 1$ s

We further proceed to compare the closed form solutions with the outcomes of three-dimensional numerical simulations carried out using the finite-element software Comsol Multiphysics [45]. The objective of this analysis was to assess the validity of the approximate deformation forms (4.1)–(4.2) used to derive the closed form expression of the evolution equation for varying specimen geometries and deformation rates. The details of the numerical implementation are given in appendix A, whereas the geometry of the specimen and the details of the mesh are shown in figure 6. For all simulations, it was assumed that $L = W$, i.e. the specimen has a square cross-section in the $\mathbf{e}_2 - \mathbf{e}_3$ plane. The discretization was carried out with 1.700 tetrahedral elements corresponding to 15.300 degrees of freedom. To simulate the simple shear experiment, the bottom face of the specimen was clamped, such that the displacement is zero $\mathbf{u} = \mathbf{0}$, whereas the top face was displaced such that $\mathbf{u} = H\,\gamma(t)\,\mathbf{e}_1$. The geometric and constitutive parameters used in the FE simulations are listed in table 2 and kept constant for all simulations except were noted.

The results of the three-dimensional numerical simulations are displayed in figures 7 and 8 for two different ratio between material to deformation times $\tau_m/\tau_d = 1$ and $\tau_m/\tau_d = 10$, in terms of

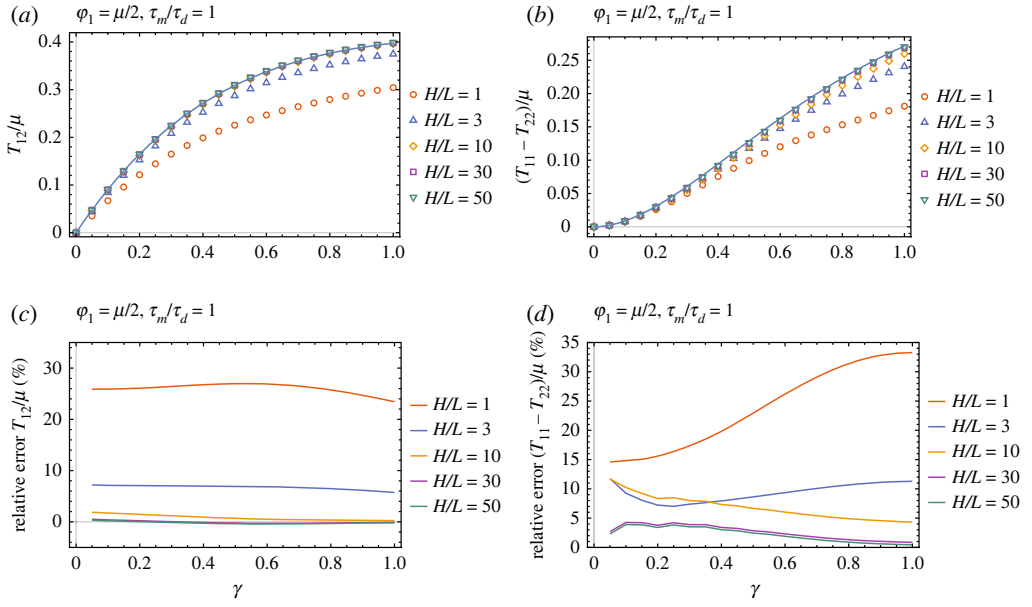

Figure 7. Comparison of three-dimensional FEM solutions for various specimen aspect ratios $H/L = \{1, 3, 10, 30, 50\}$ with the model prediction (continuous line) in a constant shear rate test with $\tau_m/\tau_d = 1$ and Neo-Hooke elastic energy. (*a*,*b*) Shear stress and normal stress difference. (*c*,*d*) The relative error between the model prediction and the FE simulations.

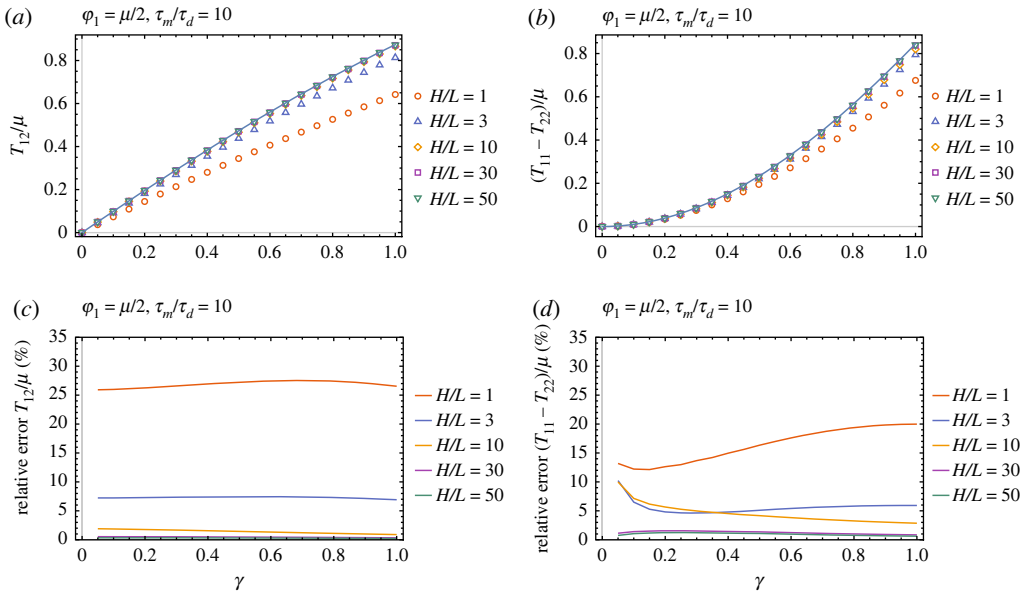

Figure 8. Comparison of three-dimensional FEM solutions for various specimen aspect ratios $H/L = \{1, 3, 10, 30, 50\}$ with the model prediction (continuous line) in a constant shear rate test with $\tau_m/\tau_d = 10$ and Neo-Hooke elastic energy. (*a*,*b*) Shear stress and normal stress difference. (*c*,*d*) The relative error between the model prediction and the FE simulations.

shear stress and normal stress difference computed as average over the mid-plane of the specimen (see appendix A). The aspect ratios of the specimen were varied in this range $H/L = 1, 3, 10, 30, 50$ passing from a cube $H/L = 1$ to a lamina $H/L = 50$. For both characteristic times, the results show that the closed form solution matches well the three-dimensional FE solution when the

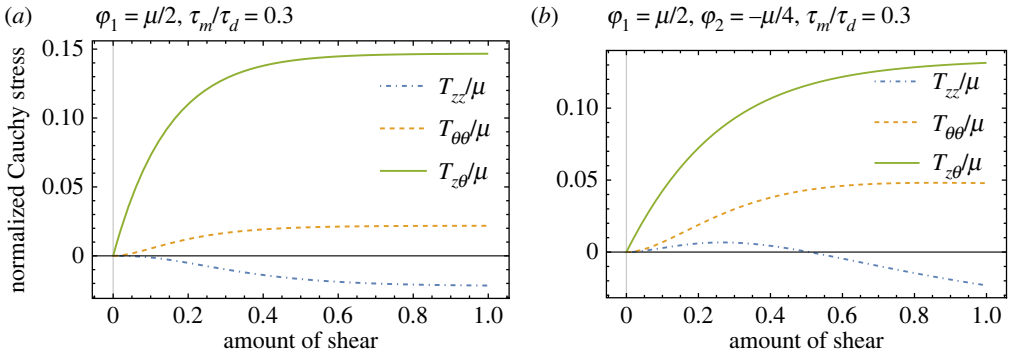

Figure 9. (Pure torsion) Normalized Cauchy stress components T_{11}/μ, T_{22}/μ and T_{12}/μ plotted as functions of the amount of shear $\gamma = \kappa\,\phi$. The results are shown for a Neo-Hooke elastic energy model in (*a*) and a Mooney–Rivlin model in (*b*). The rate parameter is set to $\tau_m/\tau_d = 0.3$.

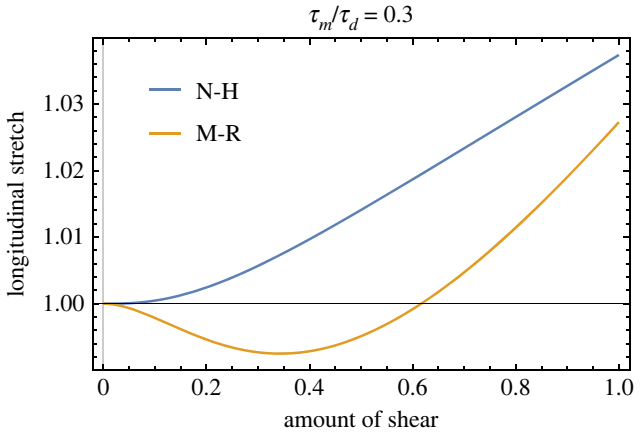

Figure 10. Longitudinal stretch λ plotted against the amount of shear $\gamma = \kappa\,\phi$ for the Neo-Hooke (N-H) and Mooney–Rivlin (M-R) material models during torsion test with free ends.

specimen aspect ratio is larger than 10. In this case, the relative error is below 5% for the shear stress and below 10% for the normal stress difference. For aspect ratios larger than 10, the degree of inhomogeneity in the three-dimensional deformation is rather limited, and the homogeneous approximation works well. For even larger aspect ratios, the error is negligible, and the prediction of the model matches that of the computationally intensive three-dimensional FE simulations.

(b) Torsion of a thin-walled cylinder

The results of the simulation concerning the pure torsion of a thin-walled cylinder are displayed in figures 9 and 10. The torsional angle is controlled in a way that the resulting shear rate is constant, i.e.

$$\phi(t) = \frac{t}{\kappa\,\tau_d}, \quad \text{s.t. } \gamma(t) = \kappa\,\phi(t) = \frac{t}{\tau_d},$$

and the height of the cylinder is kept fixed in a way that $\lambda(t) = 1$. The unknown pressure field p, necessary to evaluate the Cauchy stress, is determined by the condition of a vanishing radial stress $T_{rr} = 0$.

The results are shown in figure 9*a*,*b* in terms of the Cauchy stress components for the two previously defined material models (Neo-Hooke and Mooney–Rivlin). Interestingly the Neo-Hooke elastic energy shows that compressive longitudinal stresses arise in the cylinder due to the fixed height constraint; on the other hand the Mooney–Rivlin model displays a change of

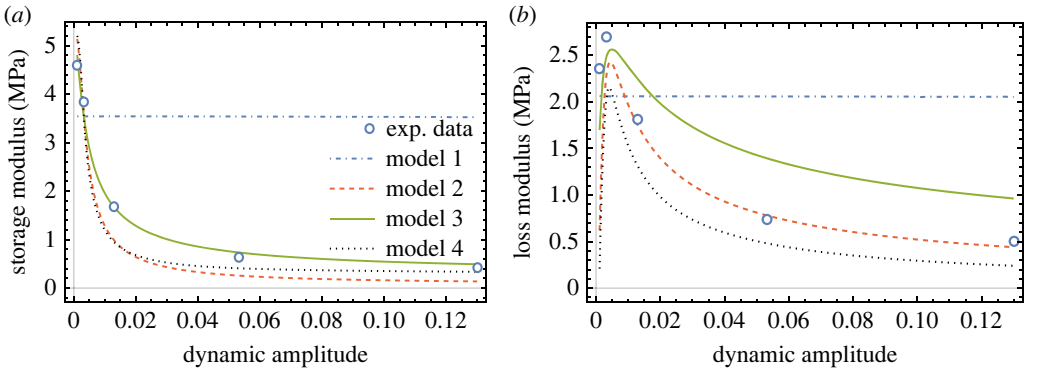

Figure 11. Performance of some of the models listed in table 1 against the experimental data on filled silicone elastomer at 1 Hz reported in [19] for storage (*a*) and loss (*b*) moduli.

the sign of the T_{zz} component which is initially positive (traction) and then become negative (compression) as the Neo-Hookean material. At very low twisting angles, both the normal stress components T_{zz} and $T_{\theta\theta}$ are quadratic functions of the twisting angle, whereas the shear stress is linear; as a consequence the cylinder is locally in a state of pure shear.

The case of cylinder free to expand longitudinally requires the determination of the additional unknown of the problem λ. This is achieved by complementing the system of evolution equations (6.5) with the algebraic equation arising from the local condition $T_{zz} = 0$. The resulting system of algebraic–differential equations can be solved by numerical integration.

The results are displayed in figure 10 in terms of longitudinal stretch λ versus amount of shear γ and confirm the behaviour observed in the pure torsion case. In the axial stretch versus amount of shear plots, interesting material behaviour is observed for the Neo-Hookean (N-H) and Mooney–Rivlin (M-R) models. For the N-H model, the cylinder exhibits a consistent expansion with increasing twist angle. This behaviour is indicative of a positive Poynting effect. By contrast, the Mooney–Rivlin model initially shows a contraction as the twist angle increases, followed by an expansion. This transient behaviour demonstrates a negative Poynting effect. The Mooney–Rivlin model's behaviour during torsion mirrors the effects observed in the simple shear tests, where the material initially was under tension before exhibiting a subsequent compression.

(c) Model calibration and comparison

To evaluate the accuracy and applicability of various models (referenced in table 1), we used experimental data from tests on filled silicone elastomers, as detailed in [19]. The experiments centred on simple shear sweep tests, where the material was subjected to a sinusoidal strain, given by $\gamma(t) = \gamma_s + \gamma_d \sin(\omega t)$. With these tests, the strain amplitude γ_d varied, while maintaining a constant frequency of 1 Hz ($\omega = 2\pi f$). During these tests, the shear stress, T_{12}, was measured. This specific test setup is frequently employed to deduce the amplitude and frequency dependence of materials akin to rubber, largely because it enables the exploration of vast amplitude and frequency domains.

The outcomes of these experiments are illustrated in figure 11, where they are characterized by storage modulus G' and loss modulus G''. These moduli are the real and imaginary components of the complex modulus $G(\omega)$, defined by

$$G' = \frac{2\omega}{N\pi}\int_0^{N\pi/\omega} \frac{T_{12}(t)}{\gamma_{\mathrm{d}}} \sin(\omega t)\mathrm{d}t \quad \text{and} \quad G'' = \frac{2\omega}{N\pi}\int_0^{N\pi/\omega} \frac{T_{12}(t)}{\gamma_{\mathrm{d}}} \cos(\omega t)\mathrm{d}t. \tag{8.1}$$

To calibrate the models in table 1, we employed a particle swarm optimization (PSO) approach facilitated by the Pymoo Python library [46]. The primary objective of this routine is to minimize

Table 3. Constitutive parameters identified from experiments for different models.

model no.	model name	parameter	value
1	Reese & Govindjee	μ_∞ (MPa)	0.10
		μ (MPa)	4.63
		η (MPa s)	4.98
2	Bergström & Boyce	μ_∞ (MPa)	0.07
		μ (MPa)	5.17
		C	−0.82
		ξ	0.14
		m	3.03
		A (MPa^{-m} s^{-1})	1.00×10^{3}
3	Kumar & Lopez-Pamies	μ_∞ (MPa)	0.27
		μ (MPa)	5.18
		η_∞ (MPa s)	5.47×10^{-4}
		η_0 (MPa s)	5.80×10
		β_1	6.74×10^{-3}
		β_2	0.44
		K_1 (MPa s)	4.32×10^{4}
		K_2 (MPa^{-2})	1.18×10^{6}
4	Strain Hardening Power Law	μ_∞ (MPa)	0.30
		μ (MPa)	1.11×10^{1}
		n	4.91
		A (MPa^{-n} s^{-m-1})	5.42×10^{4}
		m	0

discrepancies between experimental and predicted moduli, the latter being derived from the stresses generated by the models for various strain histories. While calibrating to the chosen material's data, it is evident that the material exhibits more viscoelastic traits than viscoplastic ones. As such, an extra energy term, dependent on the entire deformation **B**, was integrated into the model. This term is akin to a parallel spring in the suggested rheological model, critical for capturing the rubber's elastic reaction at particularly slow rates. The parameters obtained from the optimization are presented in table 3.

A noteworthy observation from the experimental data is the pronounced fluctuation in the storage modulus, marking an over tenfold change between the smallest (0.001) and largest (0.2) dynamic strain amplitudes tested. Such a characteristic is a dominant contributor to the nonlinearity seen in filled elastomers and is usually referred to as the Payne Effect.

Figure 11 highlights that Model 1 with a constant viscosity function η is not able to capture the decrease in storage and loss moduli seen in the experimental data, resulting in constant moduli with γ_d. Differently the other models use viscosity functions dependent upon strain and strain rates, leading to a more accurate representation of this modulus reduction. For Model 4 (Strain Hardening Power Law), the parameter m was set to 0 as it is customary in the literature and this reduce the number of free parameters to four. Model 2 (Bergström and Boyce) and Model 3 (Kumar and Lopez-Pamies) have the best performance in terms of absolute error reaching the lowest value of the objective function. Indeed, they are able to match accurately the transition from the values of the storage modulus from low dynamic amplitude to high dynamic amplitude.

9. Conclusion

In this paper, we have derived the simple shear solution for viscoplastic/viscoelastic material models. We demonstrated that unlike in large strain hyperelasticity where simple shear is determined by a single parameter, in inelastic models, the elastic deformation depends on three independent strains, requiring the solution of three coupled evolution equations. We emphasized the significant differences between this solution and the one sometimes used in the literature where only one independent elastic strain components is used. The derivations highlighted that the characteristics of the simple shear deformation of having equal invariants $I_1 = I_2$, is also true for the elastic invariants $I_1^e = I_2^e$, but for a very specific class of materials that have the same derivative of the elastic energy density with respect the two invariants, e.g. Mooney–Rivlin with equal constitutive coefficients.

The comparison between the model prediction and the full three-dimensional simulation carried out with finite elements provide insight into the accuracy of the closed form solutions. In particular it is shown that for specimen with length-to-thickness ratio of 10, the relative error between the model prediction and the three-dimensional solution drops below 5% for the shear stress and below 10% for the normal stress difference. For aspect ratio larger than 30, the error is practically negligible. For experimentalists, this implies that the inverse problem of identifying constitutive coefficients can be efficiently accomplished using the derived closed form solution, eliminating the need for computationally expensive three-dimensional FEM simulations.

Four of the models included in the proposed framework underwent calibration and were subject to comparative analysis using experimental data gathered from tests conducted on filled rubber. This comparative analysis demonstrated that particular models were capable of accurately replicating the observed decrease in storage and loss moduli, a phenomenon commonly known as the Payne effect.

The simple shear solution is extended to encompass a scenario where simple shear is combined with isochoric extension by investigating torsion and extension of a thin-walled cylinder. The analysis outcomes reveal a distinctive behaviour during torsion with free ends. Unlike an elastic material with the same energy function, where the height of the cylinder undergoes a continuous reduction, the cylinder experiences an initial shortening followed by an expansion. This behaviour represents a transient negative Poynting effect that can be attributed to the material's viscosity.

Data accessibility. The COMSOL model used in the paper is publicly available from the Zenodo repository: https://zenodo.org/records/10201580 [47].

Declaration of AI use. We have not used AI-assisted technologies in creating this article.

Authors' contributions. F.C.: data curation, formal analysis, investigation, visualization, writing—review and editing; J.C.: conceptualization, formal analysis, investigation, methodology, supervision, writing—original draft.

All authors gave final approval for publication and agreed to be held accountable for the work performed therein.

Conflict of interest declaration. We declare we have no competing interests.

Funding. J.C. gratefully acknowledges the support of PRIN-MIUR through the project 'a digital TWin for fracture and fatigue simulations in tYRES -TWYRES' CUP grant no. I53D23002240006. F.C. wishes to acknowledge the support of PON-MIUR 'Ricerca e Innovazione' 2014–2020, within the framework of the project 'Experimental and numerical characterization of rubber compounds at high frequency'. J.C. and F.C. wish to acknowledge the support of the Italian National Group of Mathematical Physics (GNFM-INdAM).

Appendix A. Finite-element implementation

The viscoplastic model is implemented into the finite element software Comsol Multiphysics [45] to solve a fully three-dimensional boundary value problem. All fields are defined in the Lagrangean setting, i.e. assumed to depend on the reference coordinates X, with the state variables of the problem defined by: the displacement field $\mathbf{u}$, that has three independent

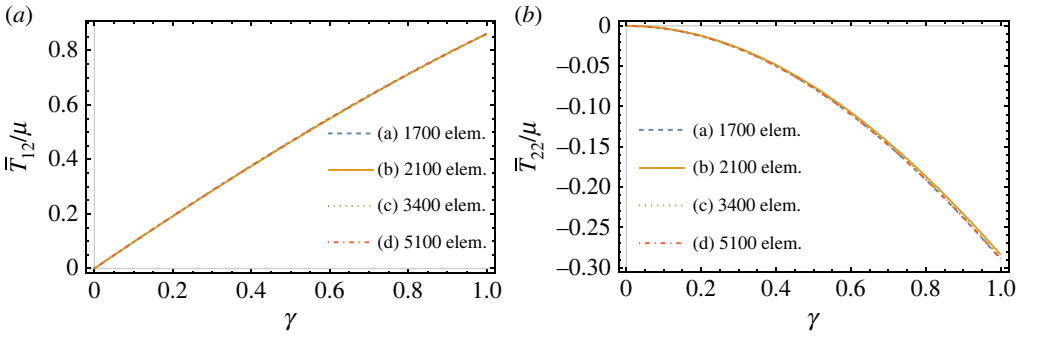

Figure 12. Effects of mesh refinement on the results for a constant shear rate test with $\dot{\gamma}_0 = 1\,\mathrm{s}^{-1}$ and constitutive parameters listed in table 2. (*a*) Shear stress, (*b*) normal stress.

components, the elastic distortional strain $\mathbf{B}_\mathrm{e}$ that has only five independent components due to the assumption $\det \mathbf{B}_\mathrm{e} = 1$, and the additional pressure field p, used to integrate separately the incompressibility constraint $\det \mathbf{F} = 1$. The weak form expression of the balance and evolution equations (integrated over the reference configuration Ω) is

$$\delta\mathcal{I}[\mathbf{u}, p, \mathbf{B}_\mathrm{e}] = \int_{\Omega_0} \left(\mathbf{S} - p\,\mathbf{F}^*\right) \cdot \nabla\delta\mathbf{u} - \int_{\Omega_0} (J-1)\,\delta p + \int_{\Omega_0} \left(\frac{1}{2}\,\mathrm{sym}(\mathbf{B}_\mathrm{e}{}^{\triangledown}\mathbf{B}_\mathrm{e}{}^{-1}) + \frac{1}{\eta(\mathbf{B}, \mathbf{B}_\mathrm{e})}\mathbf{T}'\right) \cdot \delta\mathbf{B}_\mathrm{e} \tag{A 1}$$

in which $\mathbf{S} = \mathbf{T}'\,\mathbf{F}^*$ is the first Piola–Kirchhoff stress tensor, with $\mathbf{F}^* = J\,\mathbf{F}^{-T}$, and here δ indicates the test fields. The displacement $\mathbf{u}$ is discretized thorough quadratic Lagrangean shape functions, whereas the fields p and $\mathbf{B}_\mathrm{e}$ use linear Lagrangean shape functions to avoid locking. Time differentiation was carried out with a backward differentiation scheme.

Details of the mesh are given in figure 6. The number of elements was chosen after running a convergence study whose results are shown in figure 12: for a constant shear rate test with $\dot{\gamma} = 1\,\mathrm{s}^{-1}$ increasing the number of elements over 1.700 does not produce any significant change in the results.

For all numerical simulations stresses are computed as the average over the undeformed area

$$\overline{\mathbf{T}} = \frac{1}{W\,L}\int_{\mathcal{S}_0} \mathbf{T}(X)\,\mathrm{d}X,$$

where $\mathcal{S}_0$ is the mid-plane of the specimen defined by $\mathcal{S}_0 = \{(X_1, X_2, X_3) \in \Omega\,|0 \le X_1 \le W,\ X_2 = H/2,\ 0 \le X_3 \le L\}$.

References

1. Moreira CS, Nunes LC. 2019 Effects of fiber orientation in a soft unidirectional fiber-reinforced material under simple shear deformation. *Int. J. Non-Linear Mech.* **111**, 72–81. (doi:10.1016/j.ijnonlinmec.2019.02.001)
2. Rashid B, Destrade M, Gilchrist MD. 2013 Mechanical characterization of brain tissue in simple shear at dynamic strain rates. *J. Mech. Behav. Biomed. Mater.* **28**, 71–85. (doi:10.1016/j.jmbbm.2013.07.017)
3. Sun J, Sundaresan S. 2011 A constitutive model with microstructure evolution for flow of rate-independent granular materials. *J. Fluid Mech.* **682**, 590–616. (doi:10.1017/jfm.2011.251)
4. Gent AN, Meinecke EA. 1970 Compression, bending, and shear of bonded rubber blocks. *Polym. Eng. Sci.* **10**, 48–53. (doi:10.1002/pen.760100110)
5. Upadhyay K, Bhattacharyya A, Subhash G, Spearot DE. 2019 Quasi-static and high strain rate simple shear characterization of soft polymers. *Exp. Mech.* **59**, 733–747. (doi:10.1007/s11340-019-00507-1)

6. Rivlin RS. 1948 Large elastic deformations of isotropic materials IV. further developments of the general theory. *Phil. Trans. R. Soc. Lond. A* **241**, 379–397. (doi:10.1098/rsta.1948.0024)
7. Horgan CO, Murphy JG. 2009 Simple shearing of incompressible and slightly compressible isotropic nonlinearly elastic materials. *J. Elast.* **98**, 205–221. (doi:10.1007/s10659-009-9225-1)
8. Mihai LA, Budday S, Holzapfel GA, Kuhl E, Goriely A. 2017 A family of hyperelastic models for human brain tissue. *J. Mech. Phys. Solids* **106**, 60–79. (doi:10.1016/j.jmps.2017.05.015)
9. Thiel C, Voss J, Martin RJ, Neff P. 2019 Shear, pure and simple. *Int. J. Non-Linear Mech.* **112**, 57–72. (doi:10.1016/j.ijnonlinmec.2018.10.002)
10. Horgan CO, Murphy JG. 2022 Simple shear and applied Piola-Kirchhoff shear stress. *J. Elast.* (doi:10.1007/s10659-022-09924-1)
11. Destrade M, Murphy JG, Saccomandi G. 2011 Simple shear is not so simple. *Int. J. Non-Linear Mech* **47**, 210–214. (doi:10.1016/j.ijnonlinmec.2011.05.008)
12. Destrade M, Du Y, Blackwell J, Colgan N, Balbi V. 2023 Canceling the elastic Poynting effect with geometry. *Phys. Rev. E* **107**, 1–4. (doi:10.1103/PhysRevE.107.L053001)
13. Mihai AL, Goriely A. 2013 Numerical simulation of shear and the Poynting effects by the finite element method: an application of the generalised empirical inequalities in non-linear elasticity. *Int. J. Non-Linear Mech.* **49**, 1–14. (doi:10.1016/j.ijnonlinmec.2012.09.001)
14. Horgan CO, Murphy JG. 2017 Poynting and reverse Poynting effects in soft materials. *Soft Matter* **13**, 4916ï£¡ï£¡4923. (doi:10.1039/C7SM00992E)
15. Janmey PA, McCormick ME, Rammensee S, Leight JL, Georges PC, MacKintosh FC. 2007 Negative normal stress in semiflexible biopolymer gels. *Nat. Mater.* **6**, 48–51. (doi:10.1038/nmat1810)
16. Destrade M, Horgan CO, Murphy JG. 2015 Dominant negative Poynting effect in simple shearing of soft tissues. *J. Eng. Math.* **95**, 87–98. (doi:10.1007/s10665-014-9706-5)
17. Ciambella J, Nardinocchi P. 2021 A structurally frame-indifferent model for anisotropic visco-hyperelastic materials. *J. Mech. Phys. Solids* **147**, 104247 (doi:10.1016/j.jmps.2020.104247)
18. Ciambella J, Rubin M. 2023 An elastic-viscoplastic model with non-affine deformation and rotation of a distribution of embedded fibres. *Eur. J. Mech.-A/Solids* **100**, 104985 (doi:10.1016/j.euromechsol.2023.104985)
19. Chazeau L, Brown JD, Yanyo LC, Sternstein SS. 2000 Modulus recovery kinetics and other insights into the Payne effect for filled elastomers. *Polym. Compos.* **21**, 202–222. (doi:10.1002/pc.10178)
20. Batra RC. 1992 Analysis of shear bands in simple shearing deformations of nonpolar and dipolar viscoplastic materials. *Appl. Mech. Rev.* **45**, S123–S131. (doi:10.1115/1.3121382)
21. Kim HG, Im S. 1999 Approximate analysis of a shear band in a thermoviscoplastic material. *J. Appl. Mech.* **66**, 687–694. (doi:10.1115/1.2791582)
22. Tzavaras AE. 1999 Materials with internal variables and relaxation to conservation laws. *Arch. Ration. Mech. Anal.* **146**, 129–155. (doi:10.1007/s002050050139)
23. Ghoreishy MHR. 2012 Determination of the parameters of the Prony series in hyper-viscoelastic material models using the finite element method. *Mater. Des.* **35**, 791–797. (doi:10.1016/j.matdes.2011.05.057)
24. Ghoreishy M, Firouzbakht M, Naderi G. 2014 Parameter determination and experimental verification of Bergström-Boyce hysteresis model for rubber compounds reinforced by carbon black blends. *Mater. Des.* **53**, 457–465. (doi:10.1016/j.matdes.2013.07.040)
25. Dal H, Kaliske M. 2009 Bergström-Boyce model for nonlinear finite rubber viscoelasticity: theoretical aspects and algorithmic treatment for the FE method. *Comput. Mech.* **44**, 809–823. (doi:10.1007/s00466-009-0407-2)
26. Hartmann S. 2001 Numerical studies on the identification of the material parameters of Rivlin's hyperelasticity using tension-torsion tests. *Acta Mech.* **148**, 129–155. (doi:10.1007/BF01183674)
27. Mihai LA, Goriely A. 2011 Positive or negative Poynting effect? The role of adscititious inequalities in hyperelastic materials. *Proc. R. Soc. A* **467**, 3633–3646. (doi:10.1098/rspa.2011.0281)
28. Ciambella J, Nardinocchi P. 2023 Non-affine fiber reorientation in finite inelasticity. *J. Elast.* **153**, 735–753. (doi:10.1007/s10659-022-09945-w)
29. Rubin MB, Attia A. 1996 Calculation of hyperelastic response of finitely deformed elastic-viscoplastic materials. *Int. J. Numer. Methods Eng.* **39**, 309–320. (doi:10.1002/(SICI)1097-0207(19960130)39:2<309::AID-NME858>3.0.CO;2-B)

30. Rubin M, Papes O. 2011 Advantages of formulating evolution equations for elastic-viscoplastic materials in terms of the velocity gradient instead of the spin tensor. *J. Mech. Mater. Struct.* **6**, 529–543. (doi:10.2140/jomms.2011.6.529)
31. Turzi SS. 2016 Viscoelastic nematodynamics. *Phys. Rev. E* **94**, 062705 (doi:10.1103/PhysRevE.94.062705)
32. Farina A, Fusi L, Rosso F, Saccomandi G. 2022 Creep, recovery and vibration of an incompressible viscoelastic material of the rate type: simple tension case. *Int. J. Non Linear Mech.* **138**, 103851 (doi:10.1016/j.ijnonlinmec.2021.103851)
33. Reese S, Govindjee S. 1998 A theory of finite viscoelasticity and numerical aspects. *Int. J. Solids Struct.* **35**, 3455–3482. (doi:10.1016/S0020-7683(97)00217-5)
34. Bergström J, Boyce M. 1998 Constitutive modeling of the large strain time-dependent behavior of elastomers. *J. Mech. Phys. Solids* **46**, 931–954. (doi:10.1016/S0022-5096(97)00075-6)
35. Kumar A, Lopez-Pamies O. 2016 On the two-potential constitutive modeling of rubber viscoelastic materials. *C. R. Méc.* **344**, 102–112. (doi:10.1016/j.crme.2015.11.004)
36. Hurtado J, Lapczyk I, Govindarajan S. 2013 Parallel rheological framework to model non-linear viscoelasticity, permanent set, and Mullins effect in elastomers. In *Constitutive models for rubber VIII* (eds A Gent, M Alves, M Marques), 1st ed, p. 6. London: CRC Press. (https://doi.org/10.1201/b14964)
37. Drozdov AD. 2004 Finite viscoplasticity of non-affine networks: stress overshoot under shear. *Contin. Mech. Thermodyn.* **16**, 73–95. (doi:10.1007/s00161-003-0142-4)
38. McLeish TCB, Larson RG. 1998 Molecular constitutive equations for a class of branched polymers: the pom-pom polymer. *J. Rheol.* **42**, 81–110. (doi:10.1122/1.550933)
39. Bishko G, McLeish TCB, Harlen OG, Larson RG. 1997 Theoretical molecular rheology of branched polymers in simple and complex flows: the pom-pom model. *Phys. Rev. Lett.* **79**, 2352–2355. (doi:10.1103/PhysRevLett.79.2352)
40. Kim S, Berger T, Kaliske M, Piao M. 2022 A strain rate dependent constitutive model for uncured rubber. In *Constitutive models for rubber XII* (eds J Diani, P Mazurek, N Alves), 1st edn, p. 7. London: CRC Press. (https://doi.org/10.1201/9781003310266)
41. Yoshida J, Sugiyama T. 2015 A hyperelastic visco-elasto-plastic damage model for rubber-like solids including strain-dependency of hysteretic loops. *J. Jpn. Soc. Civ. Eng. Ser, A2 (Appl. Mech. (AM))* **71**, 14–33. (doi:10.2208/jscejam.71.14)
42. Rubin MB, Chen R. 1991 Universal relations for elastically isotropic elastic-plastic materials. *J. Appl. Mech.* **58**, 283–285. (doi:10.1115/1.2897165)
43. Rajagopal KR, Wineman AS. 1987 New universal relations for nonlinear isotropic elastic materials. *J. Elast.* **17**, 75–83. (doi:10.1007/BF00042450)
44. Amin A, Lion A, Sekita S, Okui Y. 2006 Nonlinear dependence of viscosity in modeling the rate-dependent response of natural and high damping rubbers in compression and shear: experimental identification and numerical verification. *Int. J. Plast.* **22**, 1610–1657. (doi:10.1016/j.ijplas.2005.09.005)
45. Comsol Multiphysics Modeling [Online] available at: www.comsol.com/ [Accessed 19 August 2023].
46. Blank J, Deb K. 2020 pymoo: multi-objective optimization in Python. *IEEE Access* **8**, 89497–89509. (doi:10.1109/ACCESS.2020.2990567)
47. Califano F, Ciambella J. 2023 Viscoplastic simple shear at finite strains. *Zenodo*. (https://zenodo.org/records/10201580)